RSC Advances

ROYAL SOCIETY OF CHEMISTRY

www.rsc.org/advances

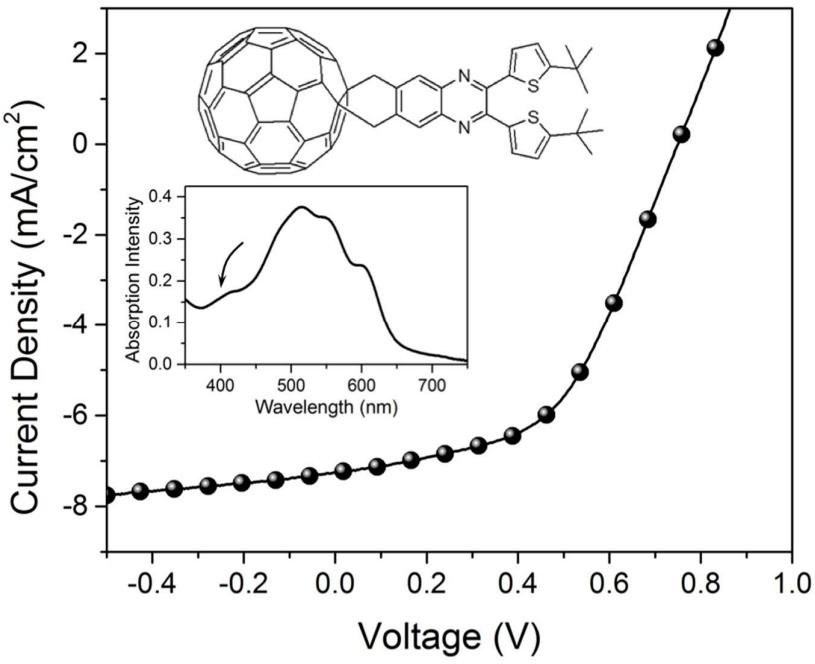

Two new quinoxaline-functionalized C_{60} derivatives with high LUMO levels have been synthesized and applied in organic solar cells. BHJ-OSCs incorporating P3HT as donor and TQMA (or TQBA) as acceptor exhibit open-circuit voltage (V_{oc}) of 0.76 V (or 0.84 V), which is about 0.12 V (or 0.20 V) higher than PCBM as electron acceptor.

Cite this: DOI: 10.1039/c0xx00000x

www.rsc.org/xxxxxx

ARTICLE TYPE

Quinoxaline-functionlized C_{60} derivatives as electron acceptors in organic solar cells

Wangqiao Chen,[a,b,†] Teddy Salim,[a,†] Haijun Fan,[a] Lewis James,[c] Yeng Ming Lam*[a] and Qichun Zhang*[a, b]

Received (in XXX, XXX) XthXXXXXXXXX 20XX, Accepted Xth XXXXXXXXX 20XX

DOI: 10.1039/b000000x

Two novel C_{60} derivative acceptors (2,3-bis(5-*tert*-butylthiophen-2-yl)-6,7-dimethylquinoxaline-C_{60}-monoadduct (**TQMA**) and 2,3-bis(5-*tert*-butylthiophen-2-yl)-6,7-dimethylquinoxaline-C_{60}-bisadduct (**TQBA**)) with high LUMO levels have been synthesized and employed as model systems to study their interactions with donor poly(3-hexylthiophene) (**P3HT**) in bulk heterojunction organic solar cells (BHJ-OSCs). The optoelectronic, electrochemistry and the subsequent photovoltaic properties of these two acceptors have been fully investigated. Although the power conversion efficiency remains to be improved, BHJ-OSCs incorporating P3HT as donor and TQMA (or TQBA) as acceptor exhibit open-circuit voltage (V_{oc}) of 0.76 V (or 0.84 V), which is about 0.12 V (or 0.20 V) higher than PCBM as electron acceptor. The different photovoltaic performance among these acceptors can be rationalized by their different LUMO energy and molecular packing.

Introduction

Organic solar cells (OSCs) have become one of the most active research areas because on top of being a clean and renewable energy source, they have other promising advantages such as simple structure, low cost, light-weight, and mechanical flexibility.[1-6] Normally, an OSC consists of a photoactive blend active layer (this layer is typically made of conjugated polymers as donors and fullerene derivatives or other molecules as acceptors), which is sandwiched between a transparent indium-tin-oxide (ITO) electrode and a low work function metal electrode. There are many factors that may affect the final power conversion efficiency (PCE) of OSCs devices, and some of the critical ones are the device structures,[7-9] morphology of active layer,[10-15] the buffer layers[16-18] and modification on the electrode.[19-22] Aside from these factors, design and synthesis of novel materials for the active layer is also extremely important and may be the most basic and efficient way to improve the device performance.

With regards to donor materials, greater successes have been witnessed in the syntheses of novel materials with broad light absorptions (narrow bandgaps), high hole mobilities, and finely-tuned electronic energy levels[17, 23-28] and some systems have already pushed the PCE to as high as 10%.[29] However, it seems that the progress in the research of new acceptors is relatively slow. Generally, the acceptors in OSCs can be divided into two groups: non-fullerene and fullerene acceptors. For the non-fullerene acceptors, there is great progress in recent years for both small molecules[30, 31] and polymers,[32-34] but the PCE is still comparatively lower compared to their fullerene counterparts (below 3%).[6, 35-36] For the fullerene acceptors, the classical acceptor is [6,6]-phenyl-C_{61}-butyric acid methyl ester ($PC_{61}BM$). Although it has been widely used in OSCs due to its high electron mobility and compatibility with various conjugated polymer/small molecule donor materials,[37] there are two obvious limitations associated with $PC_{61}BM$ compound: a) the *Lowest-Unoccupied Molecular Orbital* (LUMO) energy level of $PC_{61}BM$ is relatively low when it is used in the OSCs coupled with some conventional conjugated donor that has a fairly high *Highest-Occupied Molecular Orbital* (HOMO) energy level;[38] b) $PC_{61}BM$ has weak absorption in the visible region.

To address these problems, one strategy is to increase the LUMO energy level of the acceptor materials, which could increase the open-circuit voltage (V_{OC}) of OSCs devices since V_{OC} is strongly related to the difference between the LUMO energy level of the acceptor and the HOMO energy level of the donor.[39] Recently, a series of fullerene derivatives with higher LUMO levels than $PC_{61}BM$ have been employed as acceptors and poly(3-hexylthiophene) (P3HT) as the donor and under 1 sun illumination, and the as-fabricated OSCs give promising results with PCE > 4%. For example, Lenes et al[40, 41] used a new PCBM bisadduct (bis-$PC_{61}BM$) as acceptor and P3HT as donor in OSCs, resulting in PCE of 4.5%. Li et al[42, 43] also reported a new indene-functionalized C_{60} bisadduct (ICBA) and can reach a PCE as high as 6.5%. Other successful examples such as dihydronaphthyl-C60 bisadduct (NCBA), dihydronaphthyl-C_{70}bisadduct ($NC_{70}BA$), thieno-o-quinodimethane-C_{60} (bis-TOQC) and di(4-methylphenyl)methano-C_{60} bisadduct (DMPCBA) have also been reported.[44-48] Our group has also employed this strategy and synthesized the novel acceptor BTOQC recently.[49] The other way is to widen the absorption of the acceptor in the visible range and to enhance the whole absorption efficiency of the active layer.

For instance, $PC_{71}BM$-based OSCs usually exhibit higher PCE than $PC_{61}BM$ fabricated under similar conditions due to the stronger absorption in the visible region.[50] However, it suffers from high cost and low production yield, etc. Recently, Mikroyannidis et al[51, 52] replaced the methoxy (–OMe) group of the $PC_{61}BM$ with 4-nitro-4'-hydroxy-α-cyanostilbene and found that the PCE could be increased from 2.93% to 5.25%. Similarly, Wang et al[53] substituted methoxy group with a visible-light sensitizer **DR** to enhance the absorption of device. Unfortunately, the PCE is only 0.9%, which is much lower than that of P3HT:$PC_{61}BM$ BHJ solar cells under similar condition due to the suppression of interchain interaction of P3HT molecules in the P3HT:PCBDR blend. Through further analyzing of the above two systems, we can observe that one obvious limitation is that these new acceptors retain the basic part (PCB) of the classical PCBM acceptor and various absorption groups are introduced at the outer end of the PCBM to replace methyl group. Thus, they provide no useful information when the absorption groups are directly attached on the C_{60} molecules. With this regard, in 2012, Saravanan et al[54] reported fullerene-terthiophene (3T) dyads, which contain terthiophene synthesized *via* 1,3-dipolar cycloaddition of the corresponding azomethineylides. Although there is a contribution of 3T excitons to the photocurrent, the obtained PCE is only about 2.54%, which is still lower than that of the standard $PC_{61}BM$ system. However, it implies that the strategy is promising and it is worth to try to keep the core C_{60} unit while introducing other absorbing groups in the acceptor to enhance the total absorption of the blend film while not compromising the other device parameters.

In this work, we will explore the above-mentioned strategy through designing and synthesizing novel quinoxaline-containing fullerene derivatives, *i.e.*, 2,3-bis(5-*tert*-butylthiophen-2-yl)-6,7-dimethylquinoxaline-C_{60}-monoadduct (**TQMA**) and 2,3-bis(5-*tert*-butylthiophen-2-yl)-6,7-dimethylquinoxaline-C_{60}-bisadduct (**TQBA**) through Diels-Alder reaction. The thiophene-functionalized quinoxaline moiety in the new acceptor is directly attached on the surface of C_{60} and is thus expected to enhance the whole absorption of the device. Meanwhile, the effect of the novel acceptors on the device performance will also be investigated. For comparison, the effect of the physical blending of the quinoxaline compound with P3HT:C_{60} blends will also be presented. Our OSC device based on P3HT:TQMA exhibits a higher V_{OC} (~ 0.75 V) as compared to that of P3HT:$PC_{61}BM$ (~ 0.64 V) with a reasonable PCE of 2.80%.

RESULTS AND DISCUSSION

We employed Diels-Alder reaction as the key reaction to synthesize the target molecule[55-56] and the synthetic route of **TQMA** is shown in **Scheme 1**. 2-*tert*-Butylthiophene (R1) was synthesized according to the literature[57], which was transformed into 1,2-bis(5-*tert*-butylthiophen-2-yl)ethane-1,2-dione (R2) through double F-C reaction.[58] The 2,3-bis(5-*tert*-butylthiophen-2-yl)-6,7-dimethylquinoxaline (R3) could be obtained in almost 100% yield by reacting R2 and 4,5-dimethyl-1,2-phenylenediamine in ethanol at room temperature.[59] The 6,7-bis(bromomethyl)-2,3-bis(5-*tert*-butylthiophen-2-yl)quinoxaline (R4) was used as the precursor, which was prepared according to the literature.[60] **TQMA** and **TQBA** were prepared through the [2+4] cycloaddition reaction **between** C_{60} and the *in-situ* generated 2,3-bis(5-*tert*-butylthiophen-2-yl)-6,7-dimethene-quinoxaline.[61,62] The yield is about 35% for mono-adduct TQMA and 8% for bis-adduct TQBA.

Scheme 1 Structure and synthetic route of TQMA and TQBA

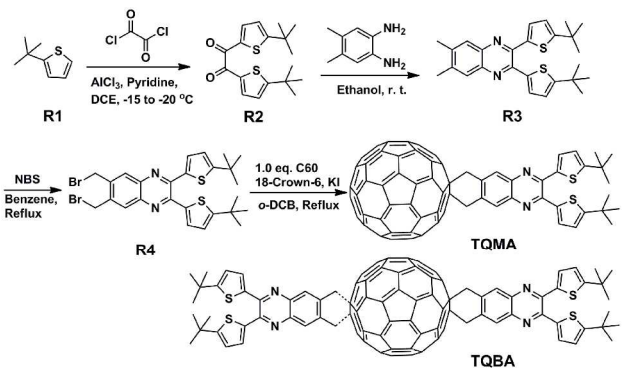

Absorption spectra of the acceptors

The spectra of the precursor R3, TQMA, TQBA and $PC_{61}BM$ are shown in **Fig. 1** for comparison purpose. For the precursor R3, there are three absorption peaks between 250 nm and 450 nm and its fluorescence appears in the range of 410 – 570 nm. Nevertheless, when R3 is attached on the surface of C_{60}, the fluorescence quenches, which indicates a possible electron transfer from the R3 to the C_{60}, suggesting its contribution to the photocurrent.[54] Consequently, TQMA and TQBA, which possess R3 groups, show apparent enhanced absorption in the 300 – 450 nm range in comparison with $PC_{61}BM$.

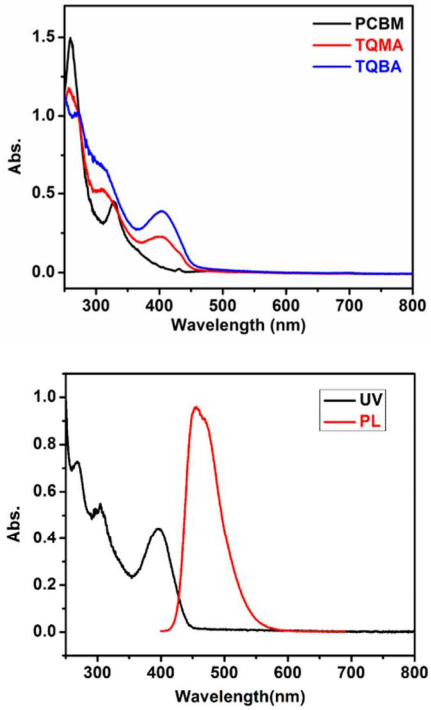

Fig. 1 UV-Vis and PL spectra of the 2,3-bis(5-*tert*-butylthiophen-2-yl)-6,7-dimethylquinoxaline (R3, top) and absorption spectra for TQMA, TQBA and $PC_{61}BM$ in chloroform (10^{-5} mol/L, bottom).

Electrochemical Properties of the acceptors

The electrochemical properties of the acceptors, which are typically studied by cyclic voltammetry (CV), are useful in estimating their respective energy levels. The LUMO energy level alignment of the acceptor, in combination with HOMO level of the donor, affects the V_{OC} of the OSCs devices and hence the final PCE because the energy levels between the donor and acceptor will have influence on the driving force of electron and hole transfer.[2] Although bisadduct fullerene derivatives have been reported to have higher V_{OC}, in certain circumstances, the monoadduct variants may also have higher V_{OC} when compared with that of classic acceptor $PC_{61}BM$.[51] **Fig. 2** shows the CV scans of R3, TQMA, TQMA as well as $PC_{61}BM$. TQMA, TQBA and $PC_{61}BM$ all exhibit three quasi-reversible reduction waves in the negative potential range from 0 to –2.0 V vs. Ag/Ag^+. On the contrary, R3 only shows one group reduction waves around –2.0 V. **Table 1** lists the half-wave potentials (defined as $E = 0.5(E_{p,c} + E_{p,a})$[63], where $E_{p,c}$ is the cathodic peak potential and $E_{p,a}$ is the corresponding anodic peak potential) of the reduction processes of the fullerene derivatives. The LUMO energy levels of the fullerene derivatives can be calculated from the onset reduction potentials (E_{red}^{on}) according to the following equation,[64]

$$E_{LUMO} = -e(E_{red}^{on} + 4.71)[eV]$$ [64]

where the unit of E_{red}^{on} is V vs. Ag/Ag^+. With this equation, the LUMO energy levels of TQMA, TQBA and $PC_{61}BM$ are calculated as –3.89, –3.76 and –3.91eV, respectively. It can be observed that the first (E_1), second (E_2) and third (E_3) reduction potentials of TQMA are almost the same as those of $PC_{61}BM$ while the onset reduction potential of TQBA is about 0.15 eV higher than that of $PC_{61}BM$. The CV data are summarized in **Table 1** and the schematics of the energy levels drawn according to the CV and UV-Vis data is depicted in **Fig. 3**. The energy level diagram shows that it is energetically favourable for the R3 excitons to be dissociated at R3/C_{60} interface due to the large Δ_{LUMO}. Nevertheless, the low LUMO level of R3 may also act as electron trap. Therefore, we firstly investigate the effects of R3 on P3HT:C_{60} blend in the following section.

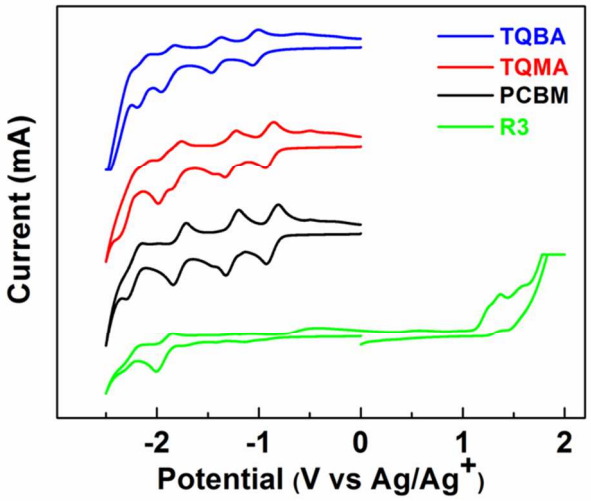

Fig. 2 Cyclic voltammograms of TQMA, TQBA and $PC_{61}BM$ in *o*-dichlorobenzene: acetonitrile (5:1 v/v) with 0.1 M Bu_4NPF_6 at 100 mV s^{-1}

Table 1. Electrochemical properties of TQMA, TQBA and $PC_{61}BM$.

Acceptor	E_1 [V]	E_2 [V]	E_3 [V]	E_{red}^{on} [V]	E_{LUMO} [eV]	E_{HOMO}^{a} [eV]	$E_g^{opt b}$ [eV]
TQMA	–0.90	–1.28	–1.81	–0.82	–3.89	–5.89	2.0
TQBA	–1.04	–1.42	–1.90	–0.95	–3.76	–5.76	2.0
$PC_{61}BM$	–0.87	–1.26	–1.78	–0.80	–3.91	–5.93	2.02
R3	–1.90			–1.80	–2.91	–5.72	2.81

[a]: $E_{HOMO} = E_{LUMO} - E_g^{opt}$, [b]: $E_g^{opt} = 1240/\lambda_{onset}$

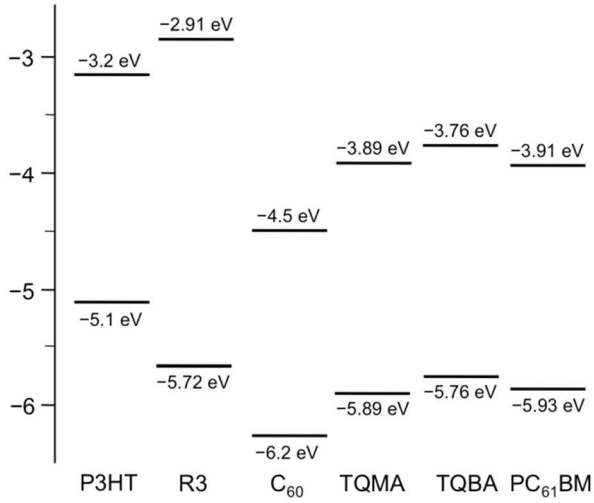

Fig. 3 Energy level schematics of the photoactive materials used in this study

The Effects of R3 on P3HT:C_{60} Blends

Fig. 4 shows the UV-Vis absorption spectra of both as-cast (NA) and thermally annealed (TA) blend films of P3HT:C_{60}. The other set of spectra with the incorporation of R3 molecules are also included for comparison. In the NA samples, the presence of R3 induces additional peak at 410 nm in the ternary P3HT:C_{60}:R3 blend spectra, which corresponds to its characteristic absorption (**Fig. 1**). Furthermore, it can also be observed that P3HT absorption between 450 and 680 nm is slightly weaker in the ternary blend as compared to its binary P3HT:C_{60} counterpart. Thermal annealing typically prompts molecular diffusion leading to self-assembly polymer backbones.[65] Consequently, both spectra of the TA blends beyond 450 nm are more intense than those of the NA blends with distinct vibronic "shoulders" at 560 and 610 nm, suggesting a heat-induced improvement in the degree of order in the blends.[66-67] Nevertheless, the characteristic absorption of R3 is no longer observed in the TA sample. It is suggested that the heat treatment might have resulted in either reorganization or conformational change of R3 molecules that alters its absorption characteristics.

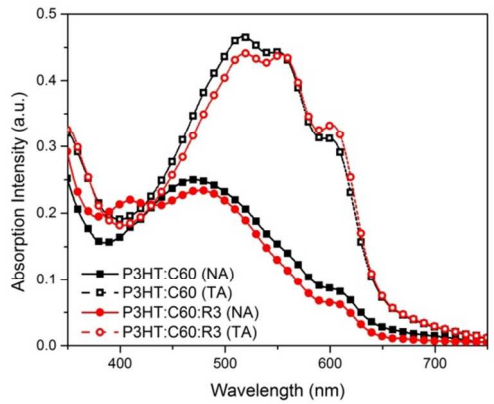

Fig. 4 UV-Vis absorption spectra of as-cast (NA) and thermally-annealed (TA) P3HT:C_{60} blend films with and without R3 incorporation.

The current density–voltage (*J–V*) characteristics under 1 sun illumination (100 mW cm^{-2}) of various P3HT:C_{60} bulk heterojunction BHJ-OSCs devices are demonstrated in **Fig. 5**(a). **Table 2** provides the summary of the corresponding device parameters extracted from the *J–V* curves. The device configuration is ITO/PEDOT:PSS/BHJ/TiOx/Al. The as-cast (NA) P3HT:C_{60} device generates short-circuit current density (J_{SC}) of 1.95 mA cm^{-2}, open-circuit voltage (V_{OC}) of 0.51 V, fill factor (FF) of 0.42 and power conversion efficiency (PCE) of 0.42%. The poor PCE is expected since as-cast device tends to have poor crystallinity, which results in poor photon harvesting and charge transport. Meanwhile, the incorporation of R3 further reduces the PCE by 6 fold to 0.07%. Although R3 has been shown to improve light absorption of P3HT:C_{60} blend (**Fig. 4**), the J_{SC} of the device decreases by more than 4 fold. This suggests that the presence of R3 molecules may have impeded the charge transport. In addition, the argument of a less efficient charge transport is also supported by the poorer FF of P3HT:C_{60}:R3 device and an increase in device series resistances (R_s) by more than 20 times. Heat treatment at 150 ºC for 20 min induces significant improvement in both J_{SC} and FF of P3HT:C_{60} to 5.64 mA cm^{-2} and 0.55, respectively. Improved photon absorption and charge transport are the primary factors of the J_{SC} increase in the TA device. As a result, the PCE of the binary device improves by more than 3 fold to 1.31%. The P3HT:C_{60}:R3 device also experiences a similar improvement in device performance, yielding a PCE of 0.66%, *i.e.* more than 9 times higher than its original as-cast device. This also shows that heat treatment is more effective to restore the degree of order in the ternary device. However, it is also expected that the presence of R3 in the thermally annealed blend will still contribute to the reduced efficiency in charge transport. This can be clearly seen from the higher R_s of the P3HT:C_{60}:R3 device (28.31 Ω cm^2) as compared to P3HT:C_{60} device (16.63 Ω cm^2). In both types of blends, thermal annealing gives rise to a reduced V_{OC}, which is itself an indication of improved blend crystallinity.

The external quantum efficiency (EQE) spectra (**Fig. 5(b)**) correspond well with both J_{SC} and PCE trends. The thermally annealed P3HT:C_{60} device generates EQE as high as 40%, which is approximately 1.7 times higher than its as-cast counterpart. On the other hand, a 5-fold improvement in EQE_{max} is obtained from P3HT:C_{60}:R3 devices upon heat treatment. The spectra also do not clearly exhibit any discernible contribution of R3 absorption, suggesting that the adverse electrical effect outweighs the improvement to its optical absorption when R3 is introduced into the P3HT:C_{60} system.

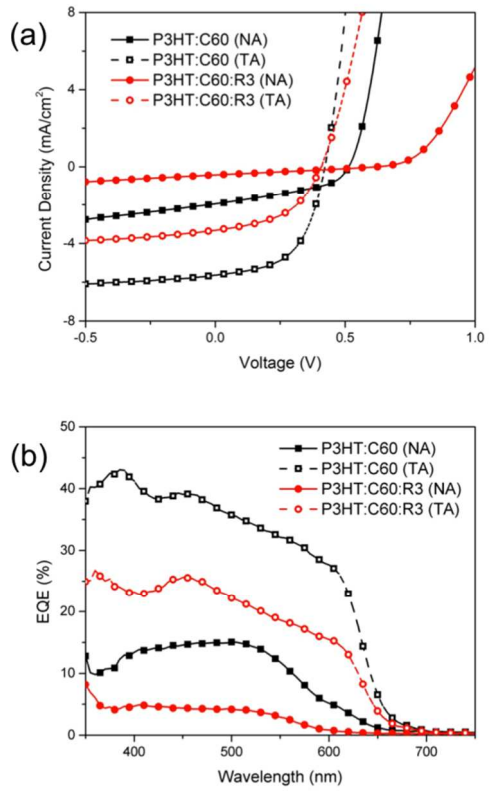

Fig. 5 (a) *J–V* characteristics and (b) EQE spectra of as-cast (NA) and thermally-annealed (TA) P3HT:C_{60} BHJ-OSC devices with and without R3 incorporation. The *J–V* characteristics were measured under AM 1.5G (100 mW cm^{-2}) illumination.

Table 2. Summary of device data of P3HT:C_{60} BHJ-OSC devices under AM 1.5G (100 mW cm^{-2}) illumination.

Blend	Annealing	J_{SC} [mA cm^{-2}]	V_{OC} [V]	FF	PCE [%]	R_s [Ω cm^2]	R_p [Ω cm^2]
P3HT:C_{60}	n/a	1.95	0.51	0.42	0.42	43.65	5.50×10^2
	150 ºC	5.64	0.42	0.55	1.31	16.63	6.08×10^2
P3HT:C_{60}:R3	n/a	0.42	0.62	0.27	0.07	889.49	1.47×10^3
	150 ºC	3.32	0.41	0.49	0.66	28.31	5.58×10^2

The blend morphology is further investigated to gain some understanding on how R3 interacts with the donor and acceptor molecules. **Fig. 6** shows a series of tapping-mode atomic force microscopy (AFM) images of both as-cast and thermally annealed P3HT:C_{60} blends with and without the incorporation of R3 molecules. The topography image of P3HT:C_{60} (NA) (**Fig. 6(a)**) reveals relatively smooth morphology with root-mean-

square roughness (σ_{RMS}) of 0.34 nm. In addition, fibrillar structures can be observed in its corresponding phase image (**Fig. 6(b)**). Upon thermal annealing at 150 ºC, the morphology of P3HT:C_{60} changes significantly following the emergence of micron-sized aggregates on the blend surface (**Fig. 6(c)**). Consequently, the blend surface roughens by a factor of 52 (σ_{RMS} = 17.90 nm). The aggregates, which appear to be clusters of smaller particles with height of < 50 nm, are often attributed to the crystallization of C_{60} molecules.[68-70] The formation of such aggregates tends to degrade device performance as they impose some limitation on the efficiency of charge collection at the electrodes. On the other hand, P3HT:C_{60}:R3 also demonstrates similarly smooth morphology prior to any heat treatment (σ_{RMS} = 0.30 nm) (Fig. **6(e)**). However, thermal annealing does not trigger the formation of any massive fullerene particles when R3 is present in the blend (Fig. **6(g)**). Hence, it is conjectured that R3 molecules are homogeneously distributed in the blend. While such homogeneous system has a significant advantage in terms of thermal stability of BHJ, it poses a crucial drawback in that the crystallization of both donor and acceptor materials may be significantly perturbed by the third blend component. As a result, charge transport will be adversely affected due to the lack of percolation pathways for both holes and electrons.

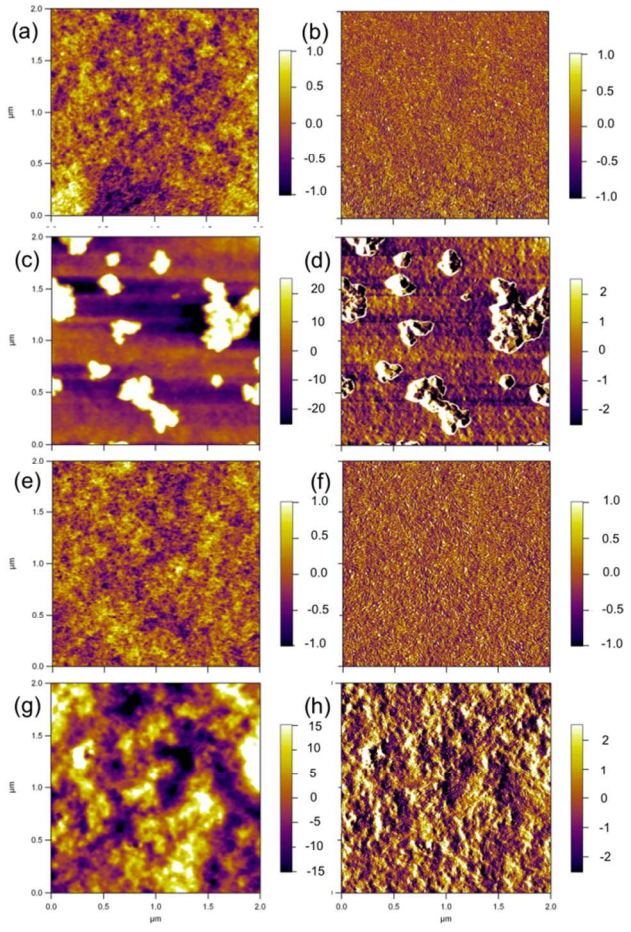

Fig. 6 Tapping-mode AFM images of: (a,b) P3HT:C_{60} (NA), (c,d) P3HT:C_{60} (TA), (e,f) P3HT:C_{60}:R3 (NA) and (g,h) P3HT:C_{60}:R3 (TA) blend films. The left images provide topography information, while the right ones reveal phase information. The scan size is 2 × 2 μm^2.

From the previous discussions, we argue that the incorporation of an additional absorbing entity into a bulk heterojunction system has remarkable potential in improving photon harvesting and hence overall device performance. Nevertheless, such system suffers from unoptimized morphological issues and presents a significant drawback in the device performance when the dopant is physically mixed with the other materials,. We infer that the lack of solubilizing group in C_{60} molecule is often thought to be the main reason of the poorer performance in OSC devices based on C_{60} as compared to its other more soluble derivatives (PCBM, etc).[71-73] Furthermore, the energy levels of this entity have to be carefully considered so that they are compatible with the main BHJ materials. In the following section, a more effective way to incorporate photoactive group, which is *via* chemical attachment of the desirable moiety onto either the donor or acceptor materials will be discussed. In this work, we explore the option of attaching the R3 precursor directly onto C_{60}, either as TQMA or TQBA, and using the modified fullerenes as alternatives to $PC_{61}BM$ for OSCs applications.

Photovoltaic Properties of P3HT:TQMA/TQBA

The UV-Vis absorption spectra of both as-cast (NA) and thermally annealed (TA) blends of P3HT and various acceptors are shown in **Fig.7**. For P3HT:TQMA and P3HT:TQBA blends, there are additional absorption "shoulders" at 410 nm reminiscence of the peak in P3HT:C_{60}:R3. These "shoulders" also correspond well with the absorption of pure TQMA and TQBA shown earlier in **Fig.1(b)**. Surprisingly, unlike the pure functionalized fullerene, P3HT:TQBA, despite having more R3 absorbing units attached to the fullerene groups, do not exhibit a stronger absorption at 410 nm in comparison to P3HT:TQMA. Therefore, P3HT:TQBA is not expected to outperform P3HT:TQMA in terms of light absorption. Comparing the spectra of all as-cast blends, P3HT absorption in P3HT:TQMA is the most blue-shifted (λ_{max} at 500 nm) with the least pronounced vibronic "shoulders" at 560 and 610 nm, followed by P3HT:$PC_{61}BM$ and P3HT:TQBA (λ_{max} at 520 nm). This indicates that the presence of TQMA results in the most prominent degree of disorder in the blend as compared to the other fullerene derivatives. In other words, it can also be expected that TQMA is the most uniformly distributed. On the other hand, the bisadduct TQBA, which exists in mixture of isomers, induces the least perturbation on the self-assembly of P3HT in the blend films. Thermal annealing promotes further molecular reorganization in the blends, which is noticeable from the bathochromic shifts in their respective absorption spectra.[65] Both P3HT:TQMA and P3HT:$PC_{61}BM$ are more susceptible to the heat treatment than P3HT:TQBA, experiencing a more extensive red-shift and an increase in absorption intensity under heating conditions. It is plausible that TQBA, being a bulkier molecule, has a more limited mass transport and hence restricted ability in restoring its crystallinity. Nevertheless, all BHJ blends exhibit similar post-heat-treatment UV-Vis absorption characteristics. The stronger absorption in the thermally annealed blends may contribute to a more efficient photon collection. Furthermore, the existence of distinct "shoulders", which are generally associated with degree of order of P3HT lamellae, also indicates the possibility of a more efficient charge transport.

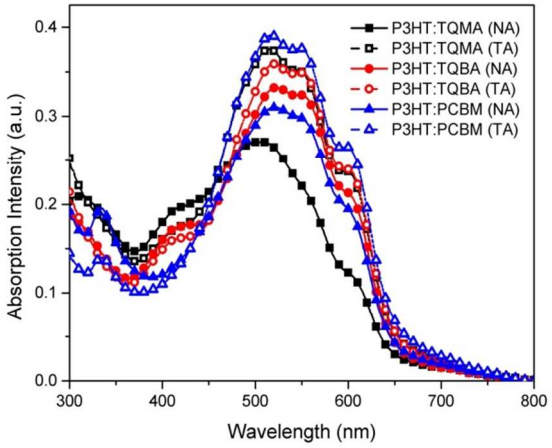

Fig. 7 UV-Vis absorption spectra of as-cast (NA) and thermally annealed (TA) blend films of P3HT with various acceptors. The donor-to-acceptor ratio is 10:6.

Despite possessing similar absorption characteristics, it is discovered that devices made with the different TA blends exhibit different properties. **Fig. 8(a)** shows the light *J*–*V* characteristics of both as-cast and thermally annealed devices fabricated with P3HT in combination with different acceptors under 1 sun illumination. The device structure used in this study is ITO/PEDOT:PSS/BHJ/TiO_x/Al. The corresponding device parameters are summarized in **Table 3**. The as-cast P3HT:TQMA device exhibits poor PCE of 0.5%, with J_{SC} of 1.84 mA cm^{-2}, V_{OC} of 0.89 V and FF of 0.31. The substandard performance of P3HT:TQMA (NA) is likely to be caused by the poor photon absorption and charge transport due to unoptimized blend morphology. However, the as-cast P3HT:TQBA device exhibits an even worse performance with PCE of 0.06%. The poor J_{SC} and FF imply that although P3HT:TQBA (NA) absorbs more light, either the photons are not effectively converted into free carriers or the charges thereof are not effectively transported across the blend film. The subsequent analysis of the R_s reveals that without any heat treatment, P3HT:TQBA has internal resistance almost 4 times as high as that of P3HT:TQMA. It is also noteworthy to point out that the V_{OC} of P3HT:TQBA (NA) is slightly lower than that of P3HT:TQMA (NA) notwithstanding the fact that TQMA has lower LUMO level than TQBA (**Table 1**). This discrepancy could be related to the morphology adopted by TQBA molecules, in which case the aggregated fullerene molecules in the blend have the possibility of lowering effective V_{OC} of the OSCs.[74] Comparing performance of the devices based on the different acceptors, the as-cast PCBM-based OSCs outperforms the rest by a huge margin with PCE of 2.71%.

Upon thermal annealing, the performance of P3HT:TQMA device improves significantly and results in J_{SC}, V_{OC}, FF and PCE of 6.2 mA cm^{-2}, 0.76 V, 0.51 and 2.4%, respectively. On the other hand, P3HT:TQBA also experiences a 6-fold improvement in device performance, mainly ascribing to the increase in J_{SC}. Similar trend of performance was also observed in the devices made without any TiO_x interlayer (*i.e.*, ITO/PEDOT:PSS/BHJ/Al); *J*–*V* curves of which are shown in ESI **Fig. S1**. However, the eventual PCE of P3HT:TQBA (TA) device is only 0.36%, which is more than 6 times lower than P3HT:TQMA (NA). The post-annealed P3HT:TQBA device still exhibits exceptionally high R_s, approximately an order of magnitude higher than the other TA devices. Even though there is not much difference between both BHJs in terms of their absorption characteristics, it is proposed that the different chemical structure of the fullerene derivatives may have caused significant variation in their electrical properties or affected the blend morphology or a combination of both. Thermal annealing seems to be more effective in generating percolation pathways for efficient hole and electron transport in P3HT:TQMA than in P3HT:TQBA. Meanwhile, the thermally annealed P3HT:PC_{61}BM device highly outperforms the remaining OSCs devices. It gives J_{SC} of 9.34 m cm^{-2}, V_{OC} of 0.64 V, FF of 0.68 and a remarkable PCE of 4.1%. It can also be observed that the V_{OC} of P3HT:TQBA (TA) is higher than that of P3HT:TQMA (TA), which now correlates well with the LUMO trend. This suggests that heat treatment may have triggered morphological change, in which reducing the degree of crystallization of TQBA at elevated temperatures as the BHJ transforms into a more thermodynamically stable system.

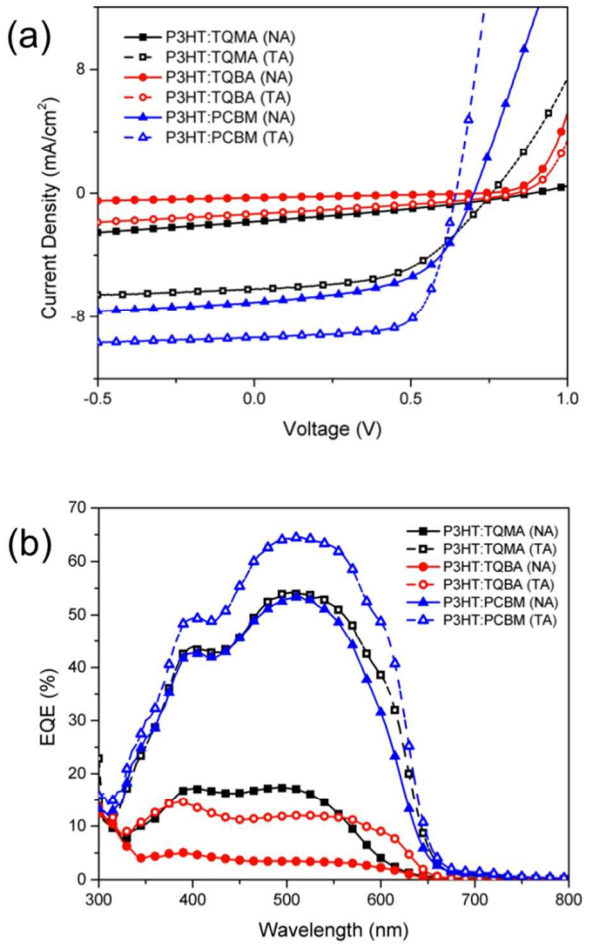

Fig. 8 (a) *J*–*V* characteristics and (b) EQE spectra of as-cast (NA) and thermally annealed (TA) P3HT BHJ-OSC devices with various acceptors. The device configuration is ITO/PEDOT:PSS/BHJ/TiO_x/Al. The *J*–*V* characteristics were measured under AM 1.5G (100 mW cm^{-2}) illumination.

Table 3. Summary of device data of P3HT BHJ-OSC devices with various acceptors under AM 1.5G (100 mW cm^{-2}) illumination.

Blend	Annealing	J_{SC} [mA cm^{-2}]	V_{OC} [V]	FF	PCE [%]	R_s [Ω cm^2]	R_p [Ω cm^2]
P3HT:TQMA	n/a	1.84	0.89	0.31	0.50	269.62	6.61×10^2
	150 ºC	6.20	0.76	0.51	2.40	40.41	1.10×10^3
P3HT:TQBA	n/a	0.29	0.72	0.26	0.06	1041.74	2.63×10^3
	150 ºC	1.34	0.84	0.32	0.36	207.75	8.80×10^2
P3HT:$PC_{61}BM$	n/a	7.06	0.70	0.55	2.71	19.48	5.86×10^2
	150 ºC	9.34	0.64	0.68	4.10	9.62	1.51×10^3

This set of data emphasizes the fact that the number of functional groups attached to fullerene molecules has crucial effect on the device properties. While most of other successful fullerene functionalization often apply the bisadduct versions for OSCs,[42, 45] our work shows that monoadduct-C_{60} may still be more beneficial if the structural issues, *e.g.*, tendency to aggregate, of the corresponding bisadduct are not fully addressed. By adding R3 into P3HT:PCBM or P3HT: TQMA blend, it may be feasible to improve the overall photon absorption and hence the device performance. However, it may have potential negative impacts on the blend morphology, which may in turn influence the charge transport properties of the active materials. In addition, adding R3 in to the devices requires an extensive amount of optimization. We will attempt to incorporate the photoactive molecule R3 in other types of established BHJ systems in our future work. In the following section, we will demonstrate the prospects of chemical attachment of absorbing units onto fullerene molecules for solar cell applications.

Fig. 8(b) shows the EQE spectra of P3HT devices fabricated with various acceptors corresponding to their *J–V* characteristics in Fig. 9(a). The trends for both EQE and J_{SC} for the different devices are similar. The thermally annealed devices of P3HT:TQMA, P3HT:TQBA and P3HT:$PC_{61}BM$ result in EQE_{max} of 54%, 15%, and 65% respectively. The lower EQE in P3HT:TQMA device as compared to P3HT:$PC_{61}BM$ could be caused by the less efficient charge transport within the polymer blend, due to either the poorer electron mobility in TQMA or less efficient percolation pathways induced by suboptimal blend morphology. To identify whether TQMA has any advantage in terms of enhanced photon absorption, the EQE spectra of P3HT:TQMA are normalized with respect to that of P3HT:$PC_{61}BM$ (ESI **Fig. S2**). It can be observed that the normalized spectra of P3HT:TQMA exhibits slightly stronger signal around 410 nm, which derives from the absorption of R3 unit in TQMA (**Fig. 8**). Therefore, it can be argued that if the electron mobility in TQMA can be improved and/or the blend morphology with TQMA as the acceptor can be optimized, it may be possible to synthesize fullerene derivatives which are more superior to the conventionally used $PC_{61}BM$.

The poor performance of P3HT:TQBA device is proposed to derive from its morphological shortcomings. **Fig. 9** demonstrates the tapping-mode AFM height images of P3HT blends with various functionalized C_{60}. The corresponding phase images are given in ESI **Fig.S3**. Both as-cast P3HT:TQMA (**Fig. 9(a)**) and P3HT:$PC_{61}BM$ (**Fig. 9(e)**) blends exhibit smooth morphology with σ_{RMS} of 0.64 and 0.39 nm, respectively. Distinct fibrillar features can be observed in both samples. Thermal annealing of these blends is expected to improve their crystallinity, which is often correlated with an increase in surface roughness, *i.e.*, σ_{RMS} = 0.96 and 0.88 nm for P3HT:TQMA (**Fig. 9(b)**) and P3HT:$PC_{61}BM$ (**Fig.9(f)**), respectively. In both types of blends, thermal annealing does not cause any significant roughening of the blend surface. As a result, these devices are not expected to suffer from poor charge extraction. On the other hand, P3HT:TQBA (**Fig. 9(c)**) adopts different morphology from that of P3HT:TQMA. While the fibrillar features can still be observed, there is a substantial roughening of the blend surface with σ_{RMS} of 3.75 nm. It is likely that the aggregation of TQBA contribute to the rougher morphology. If the acceptor molecules aggregate severely, charge dissociation will be adversely affected as there is less donor-acceptor interface. The heat treatment of P3HT:TQBA sample (**Fig. 10(d)**) reduced the surface roughening (σ_{RMS} = 2.63 nm). This suggests that the thermal diffusion of the blend molecules triggers modification of blend morphology leading to formation of fewer aggregates, which could be more desirable for OSCs. This change is believed to be the main reason behind the increase in J_{SC}, V_{OC} and FF of P3HT:TQBA device.

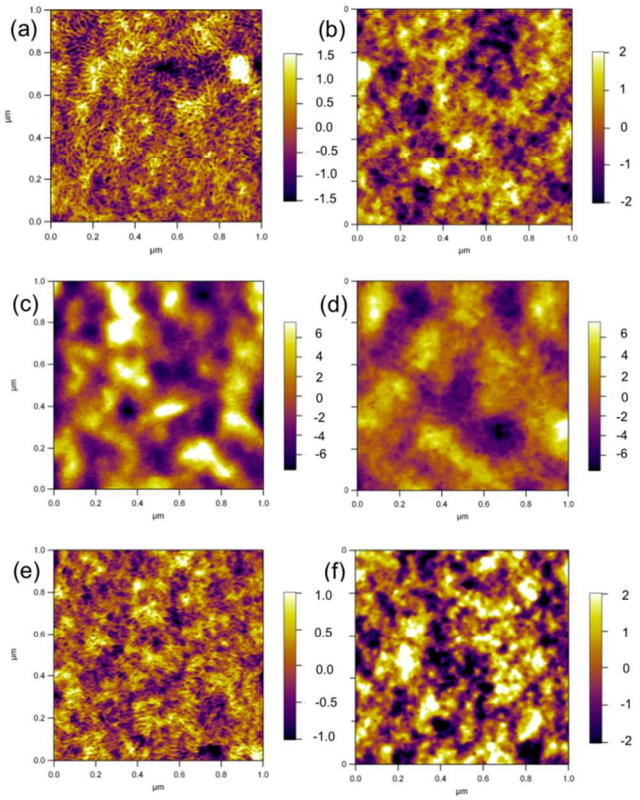

Fig. 9 Tapping-mode AFM height images of (a,b) P3HT:TQMA, (c,d) P3HT:TQBA and (e,f) P3HT:$PC_{61}BM$. The left images are those of the as-cast (NA) blends, while the right ones correspond to the thermally annealed (TA) blends. The scan size is 1 × 1 μm^2.

Even though OSCs devices made with TQBA generate poor performance, it is obvious that TQMA could be a potential alternative to $PC_{61}BM$. Therefore, P3HT:TQMA system was further optimized to expand the limit of its obtainable PCE. Following this attempt, the P3HT:TQMA devices were fabricated with blend solutions prepared in chlorobenzene (CB) with a range of different donor-to-acceptor (D:A) ratios. Chlorobenzene was chosen because its lower boiling point as compared to that of *o*-dichlorobenzene (*o*-DCB) may assist in the formation of thicker blend film, which in turn is beneficial in improving light absorption. The UV-Vis absorption spectra of P3HT:TQMA films with various D:A ratios are shown in ESI **Fig. S4**. As the amount of acceptor (TQMA) increases, the absorption "shoulder" at 410 nm expectedly also gets stronger. However, this is followed by a decrease in absorption of P3HT (480 – 700 nm) because there is less P3HT in the blend. Both light *J*–*V* characteristics and EQE spectra of the P3HT:TQMA devices are presented in ESI **Fig. S5**. **Table 4** summarizes the corresponding device properties. With the increase in acceptor loading in the blend, both J_{SC} and V_{OC} decrease monotonously. The photocurrent reduction, as observed in linear EQE drop, is associated with the decrease in P3HT absorption in the blend, which effectively lessens the amount of photons absorbed in the high wavelength region. Both fill factor and series resistance seem to improve with TQMA loading, suggesting the presence of more acceptor molecules in the blend helps to accommodate a more efficient electron transport without causing too much perturbation on the hole transport. There is also no significant variation in the surface morphology among P3HT:TQMA with different D:A ratios (ESI **Fig. S6**). A compromise between the improved charge transport and photon absorption is achieved at D:A = 10:7, yielding a J_{SC} of 7.25 mA cm^{-2}, a V_{OC} of 0.75, an FF of 0.51 and a PCE of 2.8%.

Device stability is a very important feature for future commercialization of organic solar cells. Unfortunately, we have not done any relevant experiments on device stability using our new materials. One reason is that our main aim in this work is to prove whether introducing the absorption group onto the acceptor (C_{60}) is a feasible or practical strategy to improve the PCE of the device. Another reason is that although the approach turns out to be working, the result still has much room for improvement. Hence, performing stability studies may not be very appealing at this stage. However, we will perform the stability study with the other novel acceptors should we observe significant improvement in our future devices.

Table 4. Summary of device data of P3HT:TQMA BHJ-OSC devices with different D:A ratios under AM 1.5G (100 mW cm^{-2}) illumination.

Ratio	J_{SC} [mA cm^{-2}]	V_{OC} [V]	FF	PCE [%]	R_s [Ω cm^2]	R_p [Ω cm^2]
10:6	7.76	0.77	0.42	2.50	50.32	5.89×10^2
10:7	7.25	0.75	0.51	2.80	39.60	7.33×10^2
10:8	6.98	0.74	0.50	2.60	41.06	8.31×10^2

Conclusion

In conclusion, we have demonstrated that functionalization of C_{60} with absorbing group such as quinoxaline yields a few benefits: (1) enhanced absorption attributed to the presence of additional photon harvesting moieties, (2) a more optimal morphology as compared to the physically mixed blend with quinoxaline derivatives, (3) a more compatible energetics of C_{60} derivative, lessening the likelihood for charge trapping and (4) improved solubility of C_{60}, leading to a better dispersed photoactive materials. The best device performance of this work is 2.8%, which is not very high if considering >10% efficiency of the current high level. Nevertheless, our work demonstrates that attaching quinoxaline group on the C_{60} can be a promising strategy for the development of new BHJ-OSCs acceptors. In the future. to improve the performance, one of the most straightforward strategies is to combine novel acceptors with efficient low bandgap D-A structure donor materials. To further push the result, much attention need to be paid to design and synthesis of more novel fullerene or non-fullerene acceptor with better aborption and appropriately high LUMO energy level.

Experimental section

Materials: Poly(3-hexylthiophene-2,5-diyl) (P3HT) (Sepiolid™ P200) (M_W = 20 kDa) was purchased from Rieke Metals. Phenyl-C_{60}-butyric acid methyl ester ($PC_{61}BM$) was obtained from Nano-C®. Both *o*-dichlorobenzene (*o*-DCB) and chlorobenzene were purchased from Sigma-Aldrich. Poly(3,4-ethylenedioxythiophene):poly(styrenesulfonate) (PEDOT:PSS) (P VP Al 4083) was purchased from Clevios™. 1H NMR (Bruker Avance DPX-400) spectra were recorded at 25 °C in deuterated chloroform ($CHCl_3$-d) and TMS as an internal standard.

Device Fabrication: P3HT:C_{60} blend solution was prepared by mixing P3HT (10 mg) and C_{60} (10 mg) in 1 mL of *o*-DCB. Quinoxaline R3 compound was added with the same molar ratio as C_{60} (R3:C_{60} = 1:1). Unless otherwise stated, P3HT blends with various fullerene derivatives (TQMA, TQBA or $PC_{61}BM$) were prepared in *o*-DCB (10:8 wt%). The mixtures were stirred overnight at 70 °C in an N_2 glovebox. The organic solar cell devices were fabricated on pre-patterned ITO-coated glass substrates. Initially, the substrates were sequentially cleaned by ultrasonication in DI water, acetone and isopropanol each for 15 min. Subsequently, PEDOT:PSS was spincoated at 3000 rpm for 60 s. The substrates were then baked at 140 °C for 10 min

followed by spincoating of blend solutions at 700 rpm for 120 s in N_2 environment. The blend films were annealed at 150 °C for 20 min, and were spincoated with TiO_x solution (in isopropanol). The hydrolysis of TiO_x precursors occurred in ambient for approximately 45 min. The samples were transferred to N_2 glovebox again for Al deposition (10^{-6} mbar). The active area of the device was 0.1 cm^2.

Device Measurement and Film Characterization: The current density–voltage (*J–V*) characteristics were measured in N_2 environment with Agilent 4155C Semiconductor Analyzer both in dark and under AM 1.5G illumination (100 mW cm^{-2}). The light intensity was calibrated with an NREL-calibrated silicon reference solar cell. External quantum efficiency (EQE) measurement was performed with a Merlin radiometer (Newport) under monochromatic light illumination. A calibrated silicon photodiode (Hamamatsu) was used as a reference device in counting the electrical signal generated by the devices. The film thickness was measured with a surface profilometer (Alpha Step 200, KLA-Tencor™). The optical absorption spectra were measured with a UV-Vis-NIR Spectrophotometer (UV-3600, Shimadzu). Atomic force microscopy (AFM) was performed on the blend surfaces with an Asylum Research (MFP-3D-BIO) to study the surface morphology. Electrochemical cyclic voltammetry (CV) was conducted on a CHI 660C Electrochemical Workstation. In the CV measurement, a Pt disk was used as the working electrode, Pt wire as the counter electrode, and Ag/Ag^+ electrode (0.01 M $AgNO_3$, 0.10 M Bu_4NPF_6 in acetonitrile) as the reference electrode were used in a mixed solution of *o*-dichlorobenzene: acetonitrile (5:1 v/v) with 0.1 M tetrabutylammonium hexafluorophosphate (NBu_4PF_6) at 100 mV s^{-1}.

1,2-bis(5-*tert*-butylthiophen-2-yl)ethane-1,2-dione(R2): To a solution of aluminium chloride (2.8 g, 21.0 mmol) in 1,2-DCE (10 mL) cooled down to –20 °C was added dropwise, in succession, a solution of oxalyl chloride (0.54 g, 4.3 mmol) in 1,2-DCE (1.5 mL), a solution of 2-*tert*-butylthiophene (**R1**, 1.4 g, 10.0 mmol) and pyridine (0.79 g, 10.0 mmol) in 1,2-DCE (3 mL). After keeping the mixture for 20 minutes between –20 °C and –15 °C, the temperature was raised to 0 °C and the mixture was poured over ice and extracted with methylene chloride. The extract was washed to neutral reaction with water and dried over magnesium sulfate. After removing the solvent under reduced pressure, the residue was purified by column chromatography (eluent: hexane: ethyl acetate = 5:1) to give product as an orange solid (1.17 g, 81%). Further purification can be obtained through recrystallization (800 mg in 30 mL petroleum ether, reflux), the yield can be up to 70%. ^{1}H NMR (300 MHz, $CDCl_3$) 7.85 (d, *J*= 3.0 Hz, 2H), 6.95 (d, *J*= 3.0 Hz, 2H), 1.42 (s, 18H); ^{13}C NMR (300 MHz, $CDCl_3$) δ: 183.0, 171.3, 137.5, 135.8, 123.8, 35.5, 32.1; MALDI-TOF MS: calculated for $C_{18}H_{22}O_2S_2 + H^+$, 335.1139; found: 335.1143 (M+).

2,3-bis(5-*tert*-butylthiophen-2-yl)-6,7-dimethyl quinoxaline(R3): In a 50 ml flask, the 1,2-bis(5-*tert*-butylthiophen-2-yl)ethane-1,2-dione (**R2**, 334 mg, 1.0 mmol) and 4,5-dimethyl-1,2-phenylenediamine (163 mg, 1.2 mmol) was added subsequently. Then, 30 mL anhydrous ethanol was added and the mixture was stirred at r.t. for about 24h. During this time, large amount of the bright yellow solid would be produced in the solution. The reaction can be monitored by TLC and will complete until the dione disappears. Filtrate the solution and the bright yellow solid can be obtained (412 mg, 95%). ^{1}H NMR (300 MHz, $CDCl_3$) δ: 7.79 (s, 2H), 7.04 (d, *J*= 3.0 Hz, 2H), 6.75 (d, *J*= 3.0 Hz, 2H), 2.46 (s, 6H), 1.42 (s, 18H); ^{13}C NMR (300 MHz, $CDCl_3$) δ: 161.0, 146.0, 140.3, 139.4, 138.7, 128.6, 127.8, 122.0, 34.8, 32.4, 20.3; MALDI-TOF MS: calculated for $C_{26}H_{30}O_2S_2 + H^+$, 435.1929; found: 435.1919 (M+).

6,7-bis(bromomethyl)-2,3-bis(5-tert-butylthiophen-2-yl)quinoxaline(R4): A mixture of 2,3-bis(5-*tert*-butylthiophen-2-yl)-6,7-dimethylquinoxaline(**R3,** 434 mg, 1.0 mmol, 1.0 equiv), NBS (427 mg, 2.4 mmol, 2.4 equiv to **R3**) and PCBO (24 mg, 0.1 mmol, 0.1 equiv to **R3**) was dissolved in anhydrous benzene at reflux temperature for 6 h under an argon atmosphere. After cooling to room temperature, the solvent was removed under vacuum. Afterwards, the residual solid was purified by taking solution (PE: CH_2Cl_2 =3: 1) as the eluent through column chromatography on silica gel. Orange sticky liquid: 350 mg, 59%. ^{1}H NMR (300 MHz, $CDCl_3$)δ: 8.01 (s, 2H), 7.18 (d, *J*= 3.0 Hz, 2H), 6.75 (d, *J*= 3.0 Hz, 2H), 4.81 (s, 4H), 1.44 (s, 18H); ^{13}C NMR (300 MHz, $CDCl_3$) δ: 162.2, 147.8, 140.2, 138.1, 137.9, 131.0, 129.5, 122.3, 35.0, 32.5, 29.8; MALDI-TOF MS: calculated for $C_{26}H_{28}Br_2O_2S_2 + H^+$, 593.0118; found: 592.9991 (M+).

TQMA and TQBA: A mixture of C_{60} (306 mg, 0.43 mmol, 1 equiv), 6,7-bis(bromomethyl)-2,3-bis(5-*tert*-butylthiophen-2-yl)quinoxaline (**R4**, 300 mg, 0.51 mmol, 1.2 equiv to C_{60}), potassium iodide (399 mg, 2.04 mmol, 4 equiv to **R4**), and 18-crown-6 (539 mg, 2.04 mmol, 1.0 equiv to potassium iodide) was dissolved in anhydrous *o*-dichlorobenzene at reflux temperature for 48 h under an argon atmosphere in dark. After cooling to room temperature, the solvent was removed under vacuum. Afterwards, the solid was transferred into methanol (10 mL × 3), sonicated and centrifuged. The residual solid was purified by taking toluene as the eluent through column chromatography on silica gel. The separated monoadduct TQMA was 170 mg, yield, 35%. ^{1}H-NMR (300 MHz, $CDCl_3$) δ: 8.32 (s, 2H), 7.23 (d, *J* = 3.0Hz, 2H), 6.79 (d, *J*= 3.0 Hz, 2H), 5.07 (d, *J* = 15 Hz, 2H), 4.64 (d, *J* = 15Hz, 2H), 1.46 (s, 18H). MALDI-TOF MS: calculated for $C_{86}H_{28}N_2S_2 + H^+$, 1153.1772; found: 1153.0865 (M+). Bisadduct TQBA was 51 mg, yield, 8%.^{1}H-NMR (300 MHz, $CDCl_3$) δ: 8.44–8.00 (m, 4H), 7.32–7.11 (m, 4H), 6.82–6.69 (m, 4H), 5.30–4.01 (m, 8H), 1.57–1.41 (m, 36H); MALDI-TOF MS: calculated for $C_{112}H_{56}O_4S_4 + H^+$,1585.34; found: 1585.33.

Acknowledgement

Q.Z. thanks the financial support from AcRF Tier 1 (RG 16/12) from MOE, MOE Tier 2 (ARC 20/12 and ARC 2/13), and CREATE program (Nanomaterials for Energy and Water Management) from NRF, Singapore

Notes and references

[a]*School of Materials Science and Engineering, Nanyang Technological University, 50 Nanyang Avenue, Singapore 639798. Email: YMLam@ntu.edu.sg; qczhang@ntu.edu.sg*
[b]*Institute for Sports Research, Nanyang Technological University, 50 Nanyang Avenue, Singapore 639798*
[c]*School of Sport, Exercise a nd Health Sciences, Loughborough University, Loughborough Leicestershire, LE11 3TU, UK*

†These two authors have equal contribution to this paper.

‡Electronic Supplementary Information (ESI) available: [details of any supplementary information available should be included here]. See DOI: 10.1039/b000000x/

‡ Footnotes should appear here. These might include comments relevant to but not central to the matter under discussion, limited experimental and spectral data, and crystallographic data.

References

1. S. Gunes, H. Neugebauer and N. S. Sariciftci, *Chem. Rev.*, 2007, **107**, 1324–1338.
2. B. C. Thompson and J. M. J. Frechet, *Angew.Chem. Int. Edit.*, 2008, **47**, 58–77.
3. Y. J. Cheng, S. H. Yang and C. S. Hsu, *Chem. Rev.*, 2009, **109**, 5868–5923.
4. Y. F. Li, *Acc.Chem. Res.*, 2012, **45**, 723–733.
5. Q. Zhang and X. Liu, *Small*, 2012, **8**, 3711–3713.
6. Y. Z. Lin, Y. F. Li and X. W. Zhan, *Chem. Soc. Rev.*, 2012, **41**, 4245–4272.
7. N. J. Zhou, X. G. Guo, R. P. Ortiz, S. Q. Li, S. M. Zhang, R. P. H. Chang, A. Facchetti and T. J. Marks, *Adv. Mater.*, 2012, **24**, 2242–2248.
8. J. Y. Zou, H. L. Yip, Y. Zhang, Y. Gao, S. C. Chien, K. O'Malley, C. C. Chueh, H. Z. Chen and A. K. Y. Jen, *Adv. Funct. Mater.*, 2012, **22**, 2804–2811.
9. J. Y. Kim, K. Lee, N. E. Coates, D. Moses, T. Q. Nguyen, M. Dante and A. J. Heeger, *Science*, 2007, **317**, 222–225.
10. W. L. Ma, C. Y. Yang, X. Gong, K. Lee and A. J. Heeger, *Adv. Funct.Mater.*, 2005, **15**, 1617–1622.
11. Q. Zhang, J. Xiao, Z. Y. Yin, H. M. Duong, F. Qiao, F. Boey, X. Hu, H. Zhang and F. Wudl, *Chem. Asian. J.* 2011, **6**, 856–862.
12. G. Li, V. Shrotriya, J. S. Huang, Y. Yao, T. Moriarty, K. Emery and Y. Yang, *Nat.Mater.*, 2005, **4**, 864–868.
13. A. J. Moule and K. Meerholz, *Adv. Funct.Mater.*, 2009, **19**, 3028–3036.
14. Z. Yin, S. Wu, X. Zhou, X. Huang, Q. Zhang, F. Boey and H. Zhang, *Small*, 2010, **6**, 307–309.
15. M. T. Dang, L. Hirsch, G. Wantz and J. D. Wuest, *Chem. Rev.*, 2013, **113**, 3734–3765.
16. J. H. Seo, A. Gutacker, Y. M. Sun, H. B. Wu, F. Huang, Y. Cao, U. Scherf, A. J. Heeger and G. C. Bazan, *J. Am.Chem. Soc.*, 2011, **133**, 8416–8419.
17. Z. C. He, C. M. Zhong, X. Huang, W. Y. Wong, H. B. Wu, L. W. Chen, S. J. Su and Y. Cao, *Adv.Mater.*, 2011, **23**, 4636–4643.
18. R. Po, C. Carbonera, A. Bernardi and N. Camaioni, *Energ. Environ. Sci.*, 2011, **4**, 285–310.
19. J. Qian, K. J. Jiang, J. H. Huang, Q. S. Liu, L. M. Yang and Y. L. Song, *Angew.Chem. Int. Edit.*, 2012, 51, 10351–10354.
20. *A*. K. K. Kyaw, H. Tantang, T. Wu, L. Ke, C. Peh, Z. H. Huang, X. T. Zeng, H. V. Demir, Q Zhang and X. W. Sun, *Appl. Phys. Lett.* 2011, **99**, 021107.
21. A. K. K. Kyaw, H. Tantang, T. Wu, L. Ke, J. Wei, H. V. Demir, Q. Zhang, and X. W. Sun, *J. Phys. D: Appl. Phys.* 2012, **45**, 165103.
22. H. Tantang, A. K. K. Kyaw, Y. Zhao, M. B. Chan-Park, A. I. Y. Tok, Z. Hu, L.-J. Li, X. W. Sun and Q. Zhang, *Chem. Asian J.* 2012, **7**, 541–545
23. S. C. Price, A. C. Stuart, L. Q. Yang, H. X. Zhou and W. You, *J. Am. Chem. Soc.*, 2011, **133**, 4625–4631.
24. H. J. Son, W. Wang, T. Xu, Y. Y. Liang, Y. E. Wu, G. Li and L. P. Yu, *J. Am.Chem. Soc.*, 2011, **133**, 1885–1894.
25. J. Y. Zhou, X. J. Wan, Y. S. Liu, Y. Zuo, Z. Li, G. R. He, G. K. Long, W. Ni, C. X. Li, X. C. Su and Y. S. Chen, *J. Am.Chem. Soc.*, 2012, **134**, 16345–16351.
26. J. Y. Zhou, Y. Zuo, X. J. Wan, G. K. Long, Q. Zhang, W. Ni, Y. S. Liu, Z. Li, G. R. He, C. X. Li, B. Kan, M. M. Li and Y. S. Chen, *J. Am.Chem. Soc.*, 2013, **135**, 8484–8487.
27. C. E. Small, S. Chen, J. Subbiah, C. M. Amb, S. W. Tsang, T. H. Lai, J. R. Reynolds and F. So, *Nat. Photonics*, 2012, **6**, 115–120.
28. L. T. Dou, J. B. You, J. Yang, C. C. Chen, Y. J. He, S. Murase, T. Moriarty, K. Emery, G. Li and Y. Yang, *Nat. Photonics*, 2012, **6**, 180–185.
29. J. B. You, L. T. Dou, K. Yoshimura, T. Kato, K. Ohya, T. Moriarty, K. Emery, C. C. Chen, J. Gao, G. Li and Y. Yang, *Nat. Commun.*, 2013, **4**, 1446–1455.
30. Y. Zhou, L. Ding, K. Shi, Y. Z. Dai, N. Ai, J. Wang and J. Pei, *Adv.Mater.*, 2012, **24**, 957–961.
31. F. G. Brunetti, X. Gong, M. Tong, A. J. Heeger and F. Wudl, *Angew.Chem. Int. Edit.*, 2010, **49**, 532–536.
32. Y. J. Hwang, G. Q. Ren, N. M. Murari and S. A. Jenekhe, *Macromolecules*, 2012, **45**, 9056–9062.
33. W. Y. Zhou, Z. G. Zhang, L. C. Ma, Y. F. Li and X. W. Zhan, *Sol. Energ. Mat. Sol. Cells*, 2013, **112**, 13–19.
34. Y. Liu, T. T. Larsen-Olsen, X. G. Zhao, B. Andreasen, R. R. Sondergaard, M. Helgesen, K. Norrman, M. Jorgensen, F. C. Krebs and X. W. Zhan, *Sol. Energ. Mat. Sol. Cells*, 2013, **112**, 157–162.
35. A. F. Eftaiha, J. P. Sun, I. G. Hill and G. C. Welch, *J.Mater.Chem. A*, 2014, **2**, 1201–1213.
36. C. L. Chochos, N. Tagmatarchis and V. G. Gregoriou, *Rsc. Adv.*, 2013, **3**, 7160–7181.
37. Y. J. He and Y. F. Li, *Phys.Chem.Chem. Phys.*, 2011, **13**, 1970–1983.
38. S. Cook, H. Ohkita, Y. Kim, J. J. Benson-Smith, D. D. C. Bradley and J. R. Durrant, *Chem. Phys. Lett.*, 2007, **445**, 276–280.
39. C. J. Brabec, A. Cravino, D. Meissner, N. S. Sariciftci, T. Fromherz, M. T. Rispens, L. Sanchez and J. C. Hummelen, *Adv. Funct.Mater.*, 2001, **11**, 374–380.
40. M. Lenes, G. J. A. H. Wetzelaer, F. B. Kooistra, S. C. Veenstra, J. C. Hummelen and P. W. M. Blom, *Adv.Mater.*, 2008, **20**, 2116–2119.
41. M. Lenes, S. W. Shelton, A. B. Sieval, D. F. Kronholm, J. C. Hummelen and P. W. M. Blom, *Adv. Funct.Mater.*, 2009, **19**, 3002–3007.
42. Y. J. He, H. Y. Chen, J. H. Hou and Y. F. Li, *J. Am.Chem. Soc.*, 2010, **132**, 1377–1382.
43. G. J. Zhao, Y. J. He and Y. F. Li, *Adv.Mater.*, 2010, **22**, 4355–4358.
44. E. Voroshazi, K. Vasseur, T. Aernouts, P. Heremans, A. Baumann, C. Deibel, X. Xue, A. J. Herring, A. J. Athans, T. A. Lada, H. Richter and B. P. Rand, *J.Mater.Chem.*, 2011, **21**, 17345–17352.
45. K. H. Kim, H. Kang, S. Y. Nam, J. Jung, P. S. Kim, C. H. Cho, C. Lee, S. C. Yoon and B. J. Kim, *Chem.Mater.*, 2011, **23**, 5090–5095.
46. Y. J. Cheng, M. H. Liao, C. Y. Chang, W. S. Kao, C. E. Wu and C. S. Hsu, *Chem.Mater.*, 2011, **23**, 4056–4062.
47. C. Y. Zhang, S. Chen, Z. Xiao, Q. Q. Zuo and L. M. Ding, *Org. Lett.*, 2012, **14**, 1508–1511.
48. X. Y. Meng, W. Q. Zhang, Z. A. Tan, Y. F. Li, Y. H. Ma, T. S. Wang, L. Jiang, C. Y. Shu and C. R. Wang, *Adv. Funct.Mater.*, 2012, **22**, 2187–2193.
49. W. Q. Chen, Q. Zhang, S. Teddy, S. A. Ekahana, X. J. Wan, T. C. Sum, Y. M. Lam, A. H. H. Cheng, Y. S. Chen, Q. C. Zhang, Tetrahedron, 2014, http://dx.doi.org/10.1016/j.tet.2014.01.026
50. M. M. Wienk, J. M. Kroon, W. J. H. Verhees, J. Knol, J. C. Hummelen, P. A. van Hal and R. A. J. Janssen, *Angew.Chem. Int. Edit.*, 2003, **42**, 3371–3375.
51. J. A. Mikroyannidis, A. N. Kabanakis, S. S. Sharma and G. D. Sharma, *Adv. Funct.Mater.*, 2011, **21**, 746–755.
52. J. A. Mikroyannidis, D. V. Tsagkournos, S. S. Sharma and G. D. Sharma, *J. Phys.Chem. C*, 2011, **115**, 7806–7816.
53. M. F. Wang, E. Chesnut, Y. M. Sun, M. H. Tong, M. Guide, Y. Zhang, N. D. Treat, A. Varotto, A. Mayer, M. L. Chabinyc, T. Q. Nguyen and F. Wudl, *J. Phys.Chem. C*, 2012, **116**, 1313–1321.
54. C. Saravanan, C. L. Liu, Y. M. Chang, J. D. Lu, Y. J. Hsieh, S. P. Rwei and L. Wang, *Acs Appl. Mater. Inter.*, 2012, **4**, 6133–6141.
55. J. L. Segura and N. Martin, *Chem. Rev.*, 1999, **99**, 3199–3246.
56. S. A. Backer, K. Sivula, D. F. Kavulak and J. M. J. Frechet, *Chem.Mater.*, 2007, **19**, 2927–2929.
57. J. Nagakubo, M. Ashizawa, T. Kawamoto, A. Tanioka and T. Mori, *Phys.Chem.Chem. Phys.*, 2011, **13**, 14370–14377.
58. T. Dallos, M. Hamburger and M. Baumgarten, *Org. Lett.*, 2011, **13**, 1936–1939.
59. V. Lukes, M. Breza, D. Vegh, P. Hrdlovic, J. Krajeovic and V. Laurinc, *Synth. Met.*, 2001, **124**, 279–286.

60. R. Neidlein and D. Knecht, *Chem. Ber-Recl*, 1987, **120**, 1593–1595.
61. P. Belik, A. Gugel, J. Spickermann and K. Mullen, *Angewandte Chem.ie-International Edition in English*, 1993, **32**, 78–80.
62. U. M. FernandezPaniagua, B. M. Illescas, N. Martin and C. Seoane, *J.Chem. Soc. Perk. T 1*, 1996, 1077–1079.
63. A. Andreev, G. Matt, C. J. Brabec, H. Sitter, D. Badt, H. Seyringer and N. S. Sariciftci, *Adv.Mater.*, 2000, **12**, 629–633.
64. Q. J. Sun, H. Q. Wang, C. H. Yang and Y. F. Li, *J.Mater.Chem.*, 2003, **13**, 800–806. "–4.71" refers to the energy level of Ag/Ag^+ reference electrode (0.01 M $AgNO_3$, 0.10 M Bu_4NPF_6 in acetonitrile) below the vacuum level. The value is based on experimental results. The following are the procedures on how to obtain the value of 4.71. Firstly, the energy level of ferrocene/ferrocenium (Fc/Fc^+) is assumed to be –4.8 eV below the vacuum level. This estimate is calculated on the basis of a rather crude approximation neglecting solvent effects using the standard electrode potential (E^o) for the normal hydrogen electrode (NHE) at about –4.6 eV (A. J. Bard, L. R. Faulkner, *Electrochemical Methods - Fundamentals and Applications,* Wiley, New York, p. 634) on the zero vacuum level scale and a value of 0.2 V vs. NHE for the potential of ferrocene/ferrocenium (Fc/Fc^+) (in acetonitrile, see: H.-M. Koepp, H. Wendt, H. Strehlow, *2. Electrochem.* 1960**, 64,** 483.) From reference: *Adv. Mater.* 1995, **7**, 551–554
Secondly, the formal potential of Fc/Fc^+ was measured as 0.09 V against Ag/Ag^+, thus, $–4.8 + 0.09 = –4.71$ eV
For more details, see reference: *Adv. Mater.* 2011, **23**, 2367–2371
65. E. Verploegen, R. Mondal, C. J. Bettinger, S. Sok, M. F. Toney and Z. A. Bao, *Adv. Funct.Mater.*, 2010, **20**, 3519–3529.
66. V. Shrotriya, J. Ouyang, R. J. Tseng, G. Li and Y. Yang, *Chem. Phys. Lett.*, 2005, **411**, 138–143.
67. T. Salim, L. H. Wong, B. Brauer, R. Kukreja, Y. L. Foo, Z. N. Bao and Y. M. Lam, *J.Mater.Chem.*, 2011, **21**, 242–250.
68. L. Wang, B. B. Liu, S. D. Yu, M. G. Yao, D. D. Liu, Y. Y. Hou, T. Cui, G. T. Zou, B. Sundqvist, H. You, D. K. Zhang and D. G. Ma, *Chem.Mater.*, 2006, **18**, 4190–4194.
69. A. Masuhara, Z. Q. Tan, H. Kasai, H. Nakanishi and H. Oikawa, *Jpn. J. Appl. Phys.*, 2009, **48**, 050206.
70. G. H. Lu, L. G. Li and X. N. Yang, *Small*, 2008, **4**, 601–606.
71. D. E. Motaung, G. F. Malgas, C. J. Arendse, S. E. Mavundla, C. J. Oliphant, D. Knoesen, *Sol. Energy Mat. Sol. Cells* 2009**, 93**, 1674–1680.
72. W. Liu, R. Liu, W. Wang, W. Li, W. Liu, K. Zheng, L. Ma, Y. Tian, Z. Bo, Y. Huang, *J. Phys. Chem. C* 2009**, 113**, 11385–11389
73. S.-H. Chan, C.-S. Lai, H.-L. Chen, C. Ting, C.-P. Chen, *Macromolecules* 2011**, 44**, 8886–8891
74. P. A. Troshin, H. Hoppe, J. Renz, M. Egginger, J. Y. Mayorova, A. E. Goryochev, A. S. Peregudov, R. N. Lyubovskaya, G. Gobsch, N. S. Sariciftci and V. F. Razumov, *Adv. Funct.Mater.*, 2009, **19**, 779–788.